Journal of Applied Physics

# Determining the band alignment of copper-oxide gallium-oxide heterostructures

Cite as: J. Appl. Phys. **129**, 115305 (2021); https://doi.org/10.1063/5.0036591
Submitted: 06 November 2020 • Accepted: 26 February 2021 • Published Online: 18 March 2021

S. L. Benz, M. Becker, A. Polity, et al.



Journal of Applied Physics ARTICLE scitation.org/journal/jap

# Determining the band alignment of copper-oxide gallium-oxide heterostructures

Cite as: J. Appl. Phys. **129**, 115305 (2021); doi: 10.1063/5.0036591
Submitted: 6 November 2020 · Accepted: 26 February 2021 ·
Published Online: 18 March 2021



S. L. Benz,[1,2,a)] M. Becker,[1,2] A. Polity,[1,2] S. Chatterjee,[1,2] and P. J. Klar[1,2]

## AFFILIATIONS

[1]Institute of Experimental Physics I, Justus Liebig University Giessen, Giessen, Germany
[2]Center for Materials Research (LaMa), Justus Liebig University Giessen, Giessen, Germany

[a)]**Author to whom correspondence should be addressed:** Sebastian.L.Benz@exp1.physik.uni-giessen.de

## ABSTRACT

The copper oxides cuprite ($Cu_2O$) and tenorite (CuO) are ideal candidates for solar cells as they promise high conversion efficiencies according to the Shockley–Queisser limit. However, both cannot readily be doped n-type, thus hampering the formation of all copper oxide p–n junctions for solar cell applications. The combination of the copper oxides with gallium sesquioxide, in particular, α-$Ga_2O_3$ and β-$Ga_2O_3$, is considered to be an excellent heterojunction system for overcoming this challenge. In such a p–n junction, the p-type copper oxide layer will act as an absorber and the transparent n-type gallium sesquioxide will act as a window layer. In these devices, the band alignment at the internal interface is crucial for the device performance. Here, we study the band alignments of four different copper oxide–gallium sesquioxide heterostructures by x-ray photoelectron spectroscopy. Within the experimental margin of error, a $Cu_2O$/α-$Ga_2O_3$ heterostructure appears to offer the most favorable band alignment for photovoltaic applications.



## INTRODUCTION

The copper oxides cuprite ($Cu_2O$) and tenorite (CuO) are abundant, cheap, readily available compounds, as well as good candidates for absorbing material in photovoltaic cells considering the restraints formulated in the Shockley–Queisser limit.[1] Both materials are intrinsically p-type semiconductors, which can be modulated in conductivity and compensated to a semi-insulting state.[2–4] The combination with an n-type semiconductor as a window layer is, thus, mandatory to form a photovoltaic cell. The different gallium sesquioxide phases are ideal candidate materials, as they are intrinsically n-type, and their ultra-wide-bandgap is suitable for use in a photovoltaic diode in absorber-window geometry.[5,6] However, the band alignment of these complex hetero-junctions, which is crucial for solar cell efficiency, remains unclear. Theoretical studies on the determination of the band alignment of heterojunctions exist, but these rely on experimental data and verification.[7] A very low conduction band offset is the most favorable case in such an arrangement.

Here, we grow and investigate a series of four different nominally undoped copper oxide/gallium oxide heterostructures, namely, CuO/α-$Ga_2O_3$, CuO/β-$Ga_2O_3$, $Cu_2O$/α-$Ga_2O_3$, and $Cu_2O$/β-$Ga_2O_3$, to determine their band offsets and to identify the material combination best suited for photovoltaic applications. The valence band offsets (VBOs) are determined by x-ray photoelectron spectroscopy (XPS) applying the method introduced by Kraut *et al.*[8] The conduction band offset (CBO) is then derived by taking into account the optical bandgap derived from optical absorption spectroscopy where the bandgap energies are extracted according to Tauc's method.[9] This combination of valence band alignments and bandgap energies suggests that the combination of $Cu_2O$ and α-$Ga_2O_3$ is ideal since it yields an almost negligible conduction band offset within an experimental margin of error of about 0.1 eV.

## EXPERIMENTAL

The $Cu_xO$/$Ga_2O_3$ heterojunctions are deposited by combining two different sputtering techniques. The gallium oxide thin films are grown on sapphire substrates ("CrysTec") by ion-beam sputter deposition (IBSD) using a stoichiometric $Ga_2O_3$ target. The substrates are precleaned (washed 10 min in acetone and 5 min in methanol in an ultrasonic bath). Growth details are described elsewhere.[10,11] These samples are then transferred to a radio-frequency (rf) sputtering apparatus, where the copper oxide thin films are deposited on top of the $Ga_2O_3$ layer using an elemental Cu target,

sputtered with a working gas mixture of Ar and O. The composition of the copper oxide layers is adjusted by tuning the $O_2$ flux, while keeping the Ar flux constant. The growth parameters are given in the supplementary material.

The phase purity and crystallites' orientations of the films of the deposited heterostructures are identified by wide-angle x-ray diffraction measurements (XRD) in Bragg–Brentano geometry using the $K_\alpha$-line of a copper anode in the 2-theta range from 15° to 80° in 0.05° steps.

The surfaces of the reference samples are investigated with a scanning electron microscope (SEM) (Zeiss Merlin series) to determine crystallite size and surface smoothness using an In-lens detector.

The x-ray photoelectron spectroscopy (XPS) measurements are conducted on a PHI Versaprobe II spectrometer at room temperature. The monochromized Al-$K_\alpha$ (1486.6 eV) x-ray anode provides the excitation at 45° to the surface normal. A depth profile with low energy resolution (0.8 eV) but high spatial resolution has been created to determine the etching routine for each sample. Thus, a high spatial resolution at the interface and low spatial resolution at the bulk material for a second measurement with higher energy resolution (0.1 eV) on the same sample is established. The detail spectra of the core levels are recorded with a pass energy of 23.5 eV and an energy resolution of 0.1 eV, while survey spectra are acquired with a pass energy of 93.5 eV and an energy resolution of 0.8 eV. In each etching step, the detail spectra of O 1s, C 1s, Ga 2p, Ga 3d, Ga 3p, Cu 2p, and Cu 3p are recorded as well as the valence band edge with high energy resolution (0.1 eV). Charge neutralization is achieved by a combination of an $Ar^+$-gun and an $e^-$-gun. The absolute energy positions of the XP spectra are post-referenced to the peak position of adventitious carbon (284.8 eV). It is worth noting that this approach might inflict considerable uncertainty in the evaluation of absolute energy values.[12] However, in this work, only the energy separation, i.e., the relative energy scales, are of interest.

The XPS data were analyzed using CasaXPS$^{TM}$ software. The relative concentrations $X_i$ of each element are obtained after correcting for the chemical sensitivity (using tabulated relative sensitivity factors $RSF_i$ of the XPS instruments' manufacturer for signal $i$) and apparatus response [transmission function $T(E)$],

$$X_i = \frac{100\, A_i}{\sum_j A_j},$$

where the intensity correction is contained in

$$A_i = \frac{I_i}{T(E)\, \lambda\, RSF_i},$$

where $I_i$ and $\lambda$ are the measured intensity of the signal $i$ and the compensation for differences in emergence path length, respectively. Energy position $E_i$ and area $A_i$ of the core level XPS signals were determined from the deconvolution using Voigt-functions with a 60% Lorentz quota. A background correction has been applied using a Shirley-background.[13] The valence band edge is fitted with a complementary error function in the bulk of each sample.[14] The valence band maximum (VBM) is then given by the intersection of the linear background on the lower binding energy side of the spectrum with the extrapolated straight line of the turning point of the complementary error function.

Optical transmission measurements are conducted on a Perkin–Elmer Lambda-900 spectrometer at room temperature with a spectral resolution of 0.5 nm. The absorption coefficient is derived directly from transmission data, assuming direct optical bandgaps for all materials investigated.

## RESULTS AND DISCUSSION

To determine reliable VBO values, one needs to investigate high purity materials at a sufficiently sharp interface. Therefore, each heterojunction's quality has to be assessed prior to the VBO determination.

Figure 1 shows characteristic XRD patterns of the deposited heterojunction constituents CuO, $Cu_2O$, α-$Ga_2O_3$, and β-$Ga_2O_3$ on sapphire, respectively. The XRD traces confirm that all samples are crystalline and phase pure. The CuO sample shows two significant reflections. The reflection at 35.5° may be associated with either the (002) or the (−111) planes. For rf-sputtered samples, this reflection is indicative of the (−111) orientation, as shown in a previous work by four-circle measurements.[2] The reflex at 38.5° is asymmetric. Hence, both the (111) orientation and the (200) orientation are present in our CuO material. Accordingly, the x-ray analysis reveals that the $Cu_2O$ sample contains crystallites of the two orientations (111) and (200), in accordance with previous results.[2] Both reflections are found at smaller angles compared with bulk material, which indicates the presence of tensile stress.

In contrast to the copper oxides, the β-$Ga_2O_3$ sample only shows one crystallite orientation. Besides the strong (0006) reflection of the c-plane sapphire, the (−201) orientation of β-$Ga_2O_3$ and its higher orders are present. As for $Cu_2O$, tensile strain is

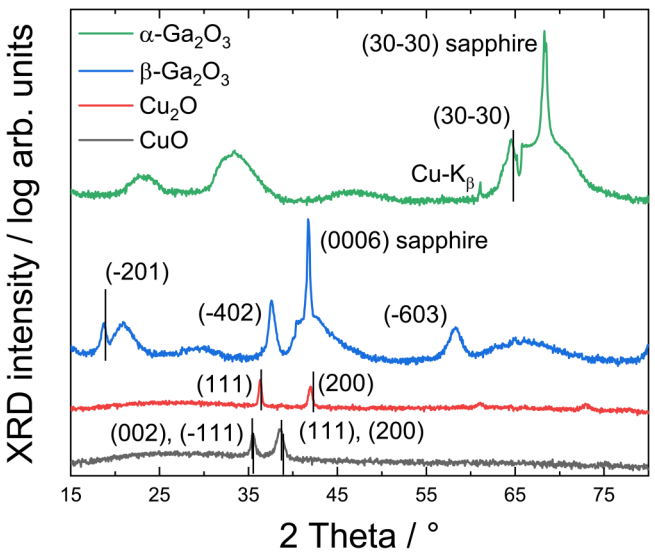


**FIG. 1.** (a) Wide-angle x-ray diffractograms of the reference samples α-$Ga_2O_3$, β-$Ga_2O_3$, $Cu_2O$, and CuO showing phase pure deposition.

apparent. The preferential (−201) orientation was also observed for the growth of β-$Ga_2O_3$ thin films by other growth methods, especially when c-cut sapphire was used as a substrate.[15–17] Besides the sharp features in the 2θ traces, a broad feature at about 21° is visible. This feature arises due to the c-plane sapphire used.[11,18]

Finally, the α-$Ga_2O_3$ sample exhibits a preferential (30–30) orientation as well as tensile strain, cf. reflection at 2θ value of about 65°. The other signals in the corresponding diffractogram arise due to the m-plane sapphire substrate. This behavior is in agreement with the findings for α-$Ga_2O_3$ grown by metalorganic chemical vapor deposition (MOCVD).[19] However, strain is not expected to compromise our results concerning the band alignment of the heterostructures, as theoretical studies have shown that, in general, the effect of strain on both the VBO and the CBO is rather small, i.e., less than 0.1 eV when compared with that on strained and unstrained heterojunctions,[20,21] which is of the same order of magnitude as the inherent uncertainty of the XPS measurements. Additional features are visible at about 23° and 33°, cf. Fig. 1, which originate from the crystalline m-plane sapphire used as substrate material.[11,18]

Figure 2 shows SEM images of the sample surfaces. The gallium oxides exhibit very smooth surfaces, promising very sharp interfaces in material stackings. The low surface roughness is typical for films grown by ion-beam sputter deposition.[10] The root mean square (RMS) roughness of the gallium oxide films is in the order of 1 nm, determined by atomic force microscopy (not shown here).

The copper oxide samples show crystallites with sizes in the order of about 100 nm. Thus, we suppose that our subsequent XPS measurements are averaged over the different crystal orientations measured in XRD as the x-ray beam of the XPS instrument has a full width at half maximum of 200 $\mu$m and the optical measurements are conducted with a millimeter-sized spot on the macroscopic scale.

To confirm the purity of the thin films, XPS survey measurements are executed at different etch depths through the entire heterojunction. Exemplarily spectra taken at different depths are shown in Fig. 3(a) for the $Cu_2O$/β-$Ga_2O_3$ heterostructure. In accordance with the measurements described above, the spectral features of the survey spectra can be entirely assigned to the materials expected in the thin films, while in the interface region, the elements of both constituent binary oxides can be found. Hence, no undesired impurities that would influence the measurements are present, e.g., those acting as additional dopants or those forming secondary phases. Looking at the core level spectra of Cu 2p and Ga 2p in Figs. 3(b) and 3(c), respectively, the phase purity of the thin films investigated is apparent, as all signals can be described with a single component. Accordingly, there is no atomic species present in the chemical environment, other than those specified by the material's stoichiometry, and none that have direct influence on the band alignment, as described by Wilson *et al.*[22] For the Cu 2p spectra, it should be noted that a weak satellite structure is present at higher binding energies that is characteristic of the $Cu_2O$ phase, and this should not be mistaken for the much stronger satellite structure that arises with the presence of CuO.[23]

Figure 3(d) finally illustrates the relative atomic concentrations of Cu, Ga, and O as a function of the etching time (corresponding to the etch depth) for the $Cu_2O$/β-$Ga_2O_3$ structure. The relative atomic concentrations seem to suggest a slight non-stoichiometry of the layers. However, this is not the case; the effect arises due to preferential etching, i.e., the two elements of the binary oxide are removed with somewhat different yields.[24,25] The compositions are determined by integrating the area of the O 1s, Cu $2p_{3/2}$, and Ga $2p_{3/2}$ signals as described in the experimental section. It can also be seen that the data taken at etching times between 6840 and 9000 s correspond to the interface region. Several data points are taken in this region. In an analog manner, corresponding graphs of the CuO/α-$Ga_2O_3$ heterojunctions are presented in Fig. 4. The survey spectra do not reveal major differences compared with the survey spectra discussed above. Nevertheless, the detail spectra of the Cu 2p region show obvious differences. Two strong satellite structures arise, which can be confidently associated with the presence of CuO.[23] The deconvolution of the main peaks exhibits two species of copper: first, one of the already mentioned CuO-phase on the higher binding energy side of the spectra and second, a lighter shaded peak that describes the presence of the $Cu_2O$ phase, introduced by the reduction of the original CuO material due to the effect of preferential sputtering caused by the etching routine utilizing the $Ar^+$-gun. This also implies that we investigate a somewhat non-stoichiometric CuO, which cannot be avoided when sputtering is used for depth profiling. Thus, the evaluation of the corresponding XPS data has to be performed very carefully. However, the Ga 2p of the α-$Ga_2O_3$ phase does not manifest any dominant differences to the β-$Ga_2O_3$ phase as theoretically predicted and experimentally verified by Swallow *et al.* just recently for MBE-grown samples investigated with XPS and Hard X-Ray Photoelectron Spectroscopy (HAXPES).[26]

Corresponding graphs for the other heterojunctions investigated are shown in the supplementary material.

The combination of the data described so far demonstrates that we acquired full datasets that are required to gain reliable information about the bulk materials as well as about the interface region of these high-quality heterojunctions.

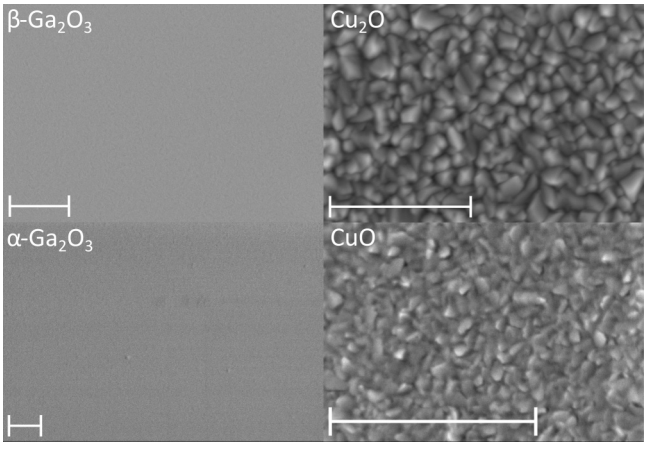


**FIG. 2.** SEM images of the reference samples' surfaces showing smooth surfaces of the gallium oxides and crystallites for the copper oxides. The white bar corresponds to a length of one 1 $\mu$m in each image.

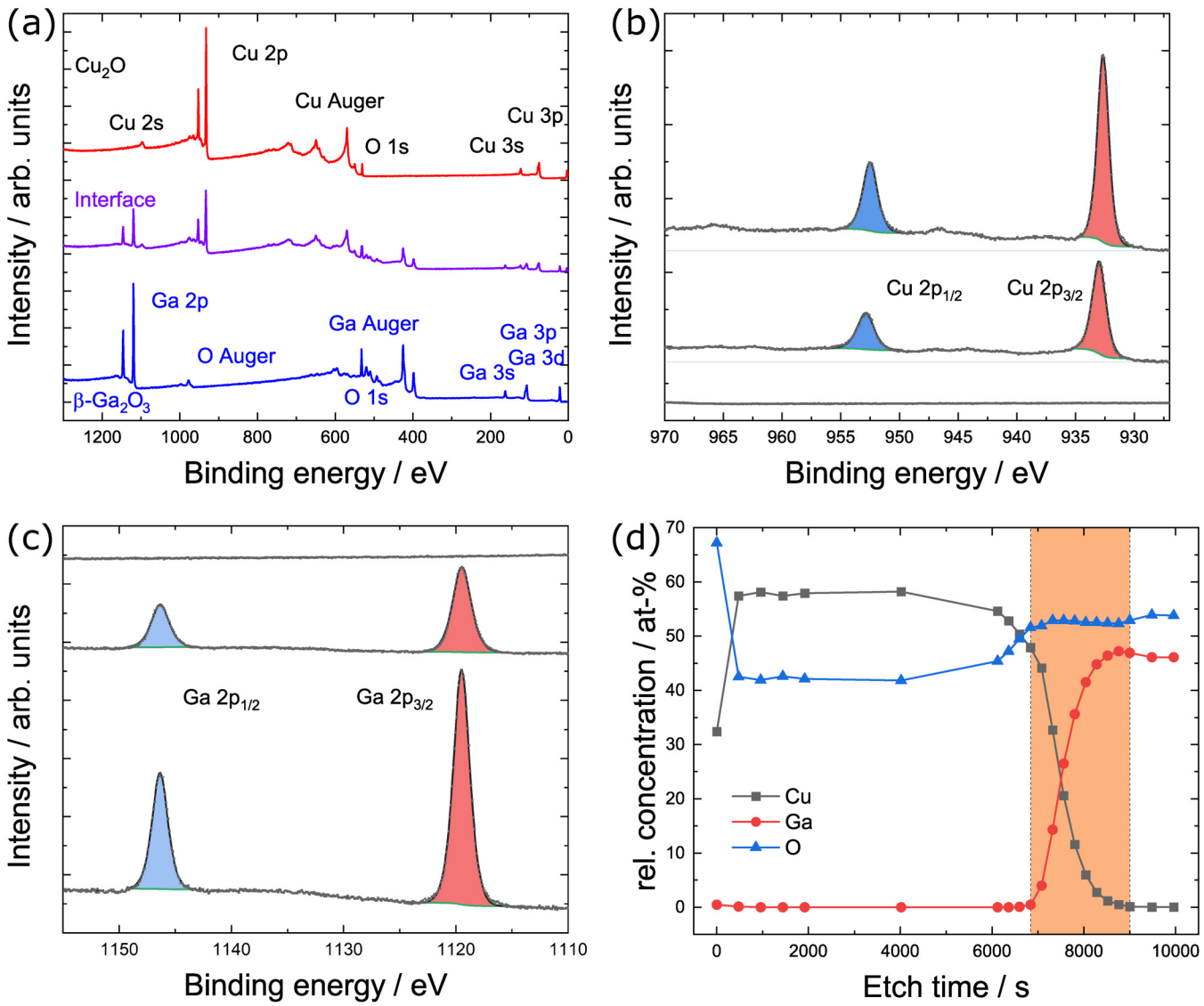


**FIG. 3.** (a) Survey XP spectra of the $Cu_2O/\beta$-$Ga_2O_3$ heterostructure at different etch depths, (b) detail spectra of the Cu 2p signals, (c) detail spectra of the Ga 2p signals (each after 480, 7560, and 9960 s of etching), and (d) the relative element concentrations of the corresponding sample as a function of etch time; the interface region is marked with orange color.

The VBO can be determined by an evaluation of the energetic core level positions and the VBM in the bulk of the two thin films and the core level positions at the heterojunction's interface region,[8]

$$\Delta E_{VB} = (E^B_{CL2} - E^B_{VB}) - (E^A_{CL1} - E^A_{VB}) - (E^I_{CL2} - E^I_{CL1}),$$

where $E^A_{CL1}$ and $E^B_{CL2}$ denote core levels 1 and 2 in the bulk materials $A$ and $B$, respectively. $E^A_{VB}$ and $E^B_{VB}$ name the positions of the VBM in the bulk of the materials $A$ and $B$, while $E^I_{CL1}$ and $E^I_{CL2}$ correspond to the positions of the core levels in the interface region. Clearly, the combination of different core level positions yields somewhat different values for the VBO. It is convenient to use various combinations of core level signals at different depths through the interface region described above, as each core level feature determined might be influenced by the chemical environment cf. chemical shifting.[27]

Here, we use the combinations of Ga 2p, Ga 3d, and Ga 3p orbital energies in combination with the Cu 2p and Cu 3p orbital energies, respectively. The relatively small energy splitting of the Ga 3d doublet is fixed for the fitting procedure to 0.45 eV according to the literature value.[28–31] Consequently, the information of

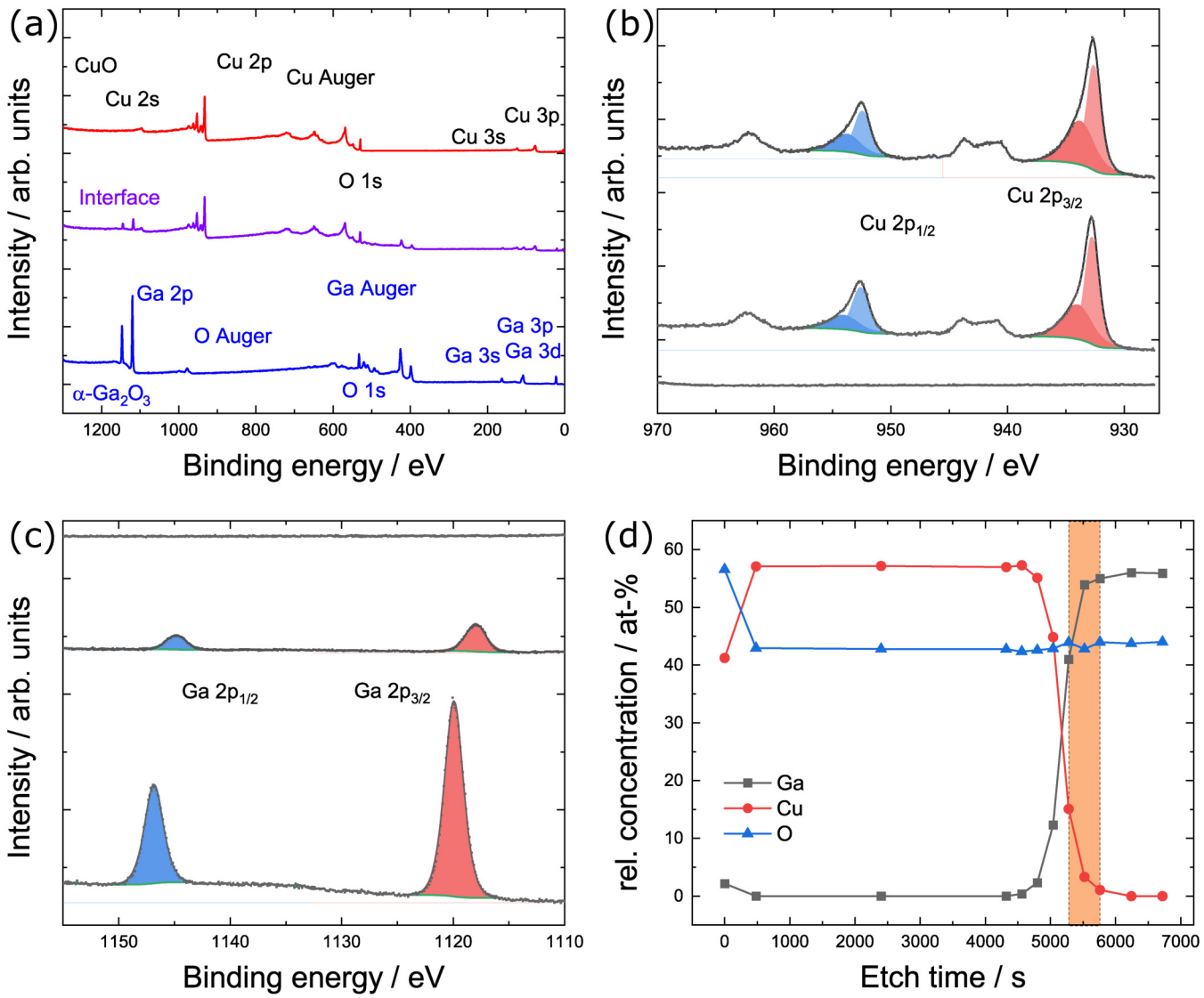


**FIG. 4.** (a) Survey XP spectra of the CuO/α-$Ga_2O_3$ heterostructure at different etch depths, (b) detail spectra of the Cu 2p signals, (c) detail spectra of the Ga 2p signals (each after 480, 5040, and 6720 s of etching), and (d) the relative element concentrations of the corresponding sample as a function of etch time; the interface region is marked with orange color.

combining the Ga $3d_{5/2}$ signal with any Cu signal is redundant with the information derived from the Ga $3d_{3/2}$ signal. Thus, we do not discuss the latter data. Additionally, we omit data related to the Cu 3p orbital as no satisfactory deconvolution of the corresponding spectra features has been possible. The lower oxidation states produced by ion-beam etching lead to additional signals [compare Fig. 4(b)]. The full width at half maximum is considerably higher for this signal compared with that of the Cu 2p signal. Therefore, it is very hard to determine the exact positions of both signals for the heterostructures containing a CuO layer. Hence, we ignore these data for better comparison of all samples.

The VBO is evaluated for each etching step and all combinations of atomic orbitals. The values are condensed into a single value as only a single VBO value is physically meaningful. The details are given in the supplementary material. Table I lists the derived VBO values.

In case the VBO is known, the CBO can be determined by adding the materials' bandgap-energy difference,

$$\Delta E_{CB} = E_g^A - E_g^B + \Delta E_{VB}.$$

**TABLE I.** Summary of results on VBOs and CBOs at 300 K.

| Sample | VBO/eV | CBO/eV |
|---|---|---|
| $CuO/\alpha\text{-}Ga_2O_3$ | $3.81 \pm 0.11$ | $-0.33 \pm 0.11$ |
| $CuO/\beta\text{-}Ga_2O_3$ | $4.20 \pm 0.03$ | $0.54 \pm 0.1$ |
| $Cu_2O/\alpha\text{-}Ga_2O_3$ | $3.21 \pm 0.06$ | $0.20 \pm 0.1$ |
| $Cu_2O/\beta\text{-}Ga_2O_3$ | $3.71 \pm 0.14$ | $1.29 \pm 0.14$ |

To derive the bandgap energies, we apply the fitting procedure suggested by Tauc *et al.*,[9] commonly used in the literature for this purpose. We anticipate direct optical bandgaps for all investigated materials, as expected from the band structure studied in the literature (Refs. 2 and 5 and references therein). The corresponding Tauc-plots are given in the supplementary material. The resulting values are shown in Table II. An overall error of 0.1 eV has been estimated. The bandgap energies found are in very good agreement with values published by other groups for the copper oxides (Ref. 2 and references therein) as well as for the gallium oxide phases (Ref. 5 and references therein).

Figure 5 summarizes all experimental data concerning the band offsets to further assess their precision. For comparison, the valence band edge of CuO of the $CuO/\alpha\text{-}Ga_2O_3$ heterostructure is set to 0 eV as a reference point. All other samples are aligned with respect to this reference, following Anderson's rule.[32,33] A comparison yields an implicit band offset for the virtual CuO/CuO heterostructures of $(0.11 \pm 0.14)$ eV summarizing both the statistical and the experimental errors. This acts as a plausibility check for the whole data set. As the virtual VBO becomes negligible, we assume a rather high reliability.

The data also allow us to derive the expected band alignment of $\alpha\text{-}Ga_2O_3$ and $\beta\text{-}Ga_2O_3$ from their heterostructures with the copper oxides. The resulting averaged VBOs are $(-0.43 \pm 0.05)$ eV for $\alpha\text{-}Ga_2O_3$ to $\beta\text{-}Ga_2O_3$ and in an analog fashion $(-0.56 \pm 0.05)$ eV for CuO to $Cu_2O$, respectively. The availability of data that can be compared with our data set is rather scarce. A range of values from 2.4[34] through 2.71 eV[35] and 3.2[36] to 3.5 eV[37] is reported for $Cu_2O/\beta\text{-}Ga_2O_3$ in the literature. This rather large range is worth discussing. It seems that the spread of values is related to the different approaches used in those studies for assessing the VBO. The values of 2.4 and 3.2 eV are derived using very similar approaches. The values given by Bae and Watahiki are solely estimates using literature values for the electron affinity and the bandgap energies of both compounds.[34,36] These values can be questioned as they rely on input data determined from different heterostructures and the validity of Anderson's rule for the band alignment, i.e., entirely neglecting interface effects. Therefore, a measurement uncertainty of more than 0.1 eV is likely as the interface properties indeed have a significant influence on the band alignment, as pointed out by Takiguchi and Miyajima[7] and Wilson *et al.*[22] for $Cu_2O$ based PV solar cells. The value of 2.71 eV given by Brandt *et al.* is also determined by XPS.[35] While the investigation is similar to our approach, the fabrication of the heterojunctions is somewhat different. In detail, Brandt *et al.* examined crystalline $Cu_2O$ grown along [111] and $Ga_2O_3$, deposited onto the $Cu_2O$ at a low deposition temperature of 120 °C. The crystalline quality of the thin film and its orientation(s) were not reported by the authors. In our samples, $Cu_2O$ preferentially exhibits (111) and (200) orientations and $\beta\text{-}Ga_2O_3$ shows a preferential (−201)-orientation, cf. Fig. 1. It is very likely that the interface discussed in Ref. 35 was different from those in our heterostructures in terms of strain and stoichiometry. This may be the reason for the discrepancy of the values determined. The value of 3.5 eV determined by Rizi *et al.* is deduced by a theoretical approach of modeling the performance of a real device.[37] Those authors also point out that the interface properties have a major influence on the band alignment. In summary, a comparison of the values reported for the $Cu_2O/\beta\text{-}Ga_2O_3$ valence band offset values is quite challenging as the deposition methods, as well as the characterization approaches, differ significantly. The value reported in this work is at the upper end of the range of the broad interval of reported values, i.e., at 3.7 eV. Thus, a satisfactorily rating cannot be given to date. Further studies, especially with complementary approaches, e.g., those aiming to use electrical measurements to

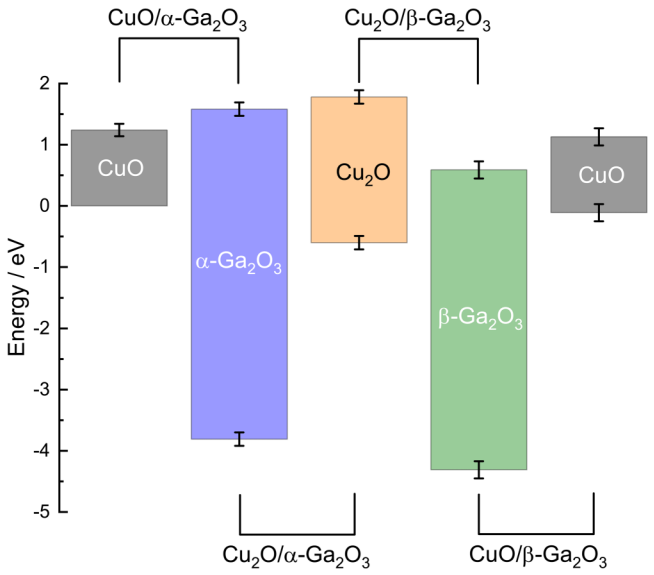


**FIG. 5.** The band alignments of all samples investigated including the bandgap energies. The VBM of CuO has been set to zero as a reference point and has, thus, no experimental uncertainty. The other materials are aligned with their errors as determined, following Anderson's rule. Consequently, the right CuO energetic position derived from the $CuO/\beta\text{-}Ga_2O_3$ heterostructure shows errors at both the valence band and the conduction band edge.

**TABLE II.** Material's bandgaps acquired with Tauc's method at 300 K.

| System | $E_g$/eV |
|---|---|
| CuO | $1.24 \pm 0.1$ |
| $Cu_2O$ | $2.38 \pm 0.1$ |
| $\beta\text{-}Ga_2O_3$ | $4.90 \pm 0.1$ |
| $\alpha\text{-}Ga_2O_3$ | $5.39 \pm 0.1$ |

obtain the heterojunction offsets, are desirable. Yet, suitable experiments so far have been reported only on heterojunctions formed by amorphous $Ga_2O_3$ films in combination with $Cu_2O$.[38,39] These studies, however, report values for the band alignment that are similar to the values determined by us for the heterojunctions between crystalline $Ga_2O_3$ and $Cu_2O$.

## CONCLUSION

We present a complete study of all four combinations of $Cu_2O$ and non-stoichiometric CuO with α-$Ga_2O_3$ and β-$Ga_2O_3$.

The study has shown that, of all four combinations, a heterojunction of $Cu_2O$ and α-$Ga_2O_3$ offers the most promising properties for application as a solar cell in absorber-window configuration. It ought to yield high solar cell efficiency as the conduction band offset becomes virtually negligible. For the production of such devices, it should be noted that the conductivity of the thin films may be controlled by extrinsic doping. As a by-product of our study, we are able to derive the virtual VBO of CuO to $Cu_2O$ as well as the virtual VBO of β-$Ga_2O_3$ to α-$Ga_2O_3$, as described in the supplementary material. The VBO of CuO to $Cu_2O$ is $(-0.56 \pm 0.05)$ eV, while the VBO of β-$Ga_2O_3$ to α-$Ga_2O_3$ is calculated to be $(-0.43 \pm 0.05)$ eV.

## SUPPLEMENTARY MATERIAL

See the supplementary material for additional notes on the growth of the materials investigated, the corresponding XP spectra of the heterostructures not shown in the main part, a mathematical description on condensing the VBO values, the determination of the optical bandgaps, a mathematical description on how the virtual band offsets were determined, and the XP spectra of the valence band maxima.

## ACKNOWLEDGMENTS

This work was funded by the Deutsche Forschungsgemeinschaft (DFG) via the RTG (Research Training Group) 2204 "Substitute Materials for sustainable Energy Technologies" and by the European Regional Development Fonts (EFRE 2DIBS). S.C. acknowledges support through the Heisenberg programs under Contract No. CH660/8.

## DATA AVAILABILITY

The data that support the findings of this study are available from the corresponding author upon reasonable request.

## REFERENCES

[1]W. Shockley and H. J. Queisser, J. Appl. Phys. **32**, 510 (1961).
[2]B. K. Meyer, A. Polity, D. Reppin, M. Becker, P. Hering, P. J. Klar, Th. Sander, C. Reindl, J. Benz, M. Eickhoff, C. Heiliger, M. Heinemann, J. Bläsing, A. Krost, S. Shokovets, C. Müller, and C. Ronning, Phys. Status Solidi B **249**, 1487 (2012).
[3]Z. Wang, P. K. Nayak, J. A. Caraveo-Frescas, and H. N. Alshareef, Adv. Mater. **28**, 3831 (2016).
[4]K. H. L. Zhang, K. Xi, M. G. Blamire, and R. G. Egdell, J. Phys.: Condens. Matter **28**, 383002 (2016).
[5]H. von Wenckstern, Adv. Electron. Mater. **3**, 1600350 (2017).
[6]S. J. Pearton, J. Yang, P. H. Cary, F. Ren, J. Kim, M. J. Tadjer, and M. A. Mastro, Appl. Phys. Rev. **5**, 011301 (2018).
[7]Y. Takiguchi and S. Miyajima, Jpn. J. Appl. Phys. **54**, 112303 (2015).
[8]E. A. Kraut, R. W. Grant, J. R. Waldrop, and S. P. Kowalczyk, Phys. Rev. B **28**, 1965 (1983).
[9]J. Tauc, R. Grigorovici, and A. Vancu, Phys. Status Solidi B **15**, 627 (1966).
[10]M. Becker, M. Gies, A. Polity, S. Chatterjee, and P. J. Klar, Rev. Sci. Instrum. **90**, 023901 (2019).
[11]M. Becker, S. L. Benz, L. Chen, A. Polity, P. J. Klar, and S. Chatterjee, J. Vac. Sci. Technol. A **38**, 063412 (2020).
[12]G. Greczynski and L. Hultman, Prog. Mater. Sci. **107**, 100591 (2020).
[13]D. A. Shirley, Phys. Rev. B **5**, 4709 (1972).
[14]F. Michel, B. Kramm, M. Becker, K. P. Hering, D. M. Hofmann, and P. J. Klar, J. Appl. Phys. **123**, 245304 (2018).
[15]E. G. Víllora, K. Shimamura, K. Kitamura, and K. Aoki, Appl. Phys. Lett. **88**, 031105 (2006).
[16]M. Orita, H. Hiramatsu, H. Ohta, M. Hirano, and H. Hosono, Thin Solid Films **411**, 134 (2002).
[17]M.-Q. Li, N. Yang, G.-G. Wang, H.-Y. Zhang, and J.-C. Han, Appl. Surf. Sci. **471**, 694 (2019).
[18]L. Spiess, G. Teichert, R. Schwarzer, H. Behnken, and C. Genzel, *Moderne Röntgenbeugung* (Springer, 2019).
[19]Y. Lv, W. Mi, C. N. Luan, and J. Ma, Adv. Mater. Res. **746**, 369 (2013).
[20]S.-H. Wei and A. Zunger, Appl. Phys. Lett. **69**, 2719 (1996).
[21]C. G. V. de Walle and J. Neugebauer, Appl. Phys. Lett. **70**, 2577 (1997).
[22]S. S. Wilson, J. P. Bosco, Y. Tolstova, D. O. Scanlon, G. W. Watson, and H. A. Atwater, Energy Environ. Sci. **7**, 3606–3610 (2014).
[23]S. Poulston, P. M. Parlett, P. Stone, and M. Bowker, Surf. Interface Anal. **24**, 811 (1996).
[24]R. V. Stuart and G. K. Wehner, J. Appl. Phys. **33**, 2345 (1962).
[25]N. Matsunami, Y. Yamamura, Y. Itikawa, N. Itoh, Y. Kazumata, S. Miyagawa, K. Morita, R. Shimizu, and H. Tawara, At. Data Nucl. Data Tables **31**, 1 (1984).
[26]J. E. N. Swallow, C. Vorwerk, P. Mazzolini, P. Vogt, O. Bierwagen, A. Karg, M. Eickhoff, J. Schörmann, M. R. Wagner, J. W. Roberts, P. R. Chalker, M. J. Smiles, P. Murgatroyd, S. A. Razek, Z. W. Lebens-Higgins, L. F. J. Piper, L. A. H. Jones, P. K. Thakur, T.-L. Lee, J. B. Varley, J. Furthmüller, C. Draxl, T. D. Veal, and A. Regoutz, Chem. Mater. **32**, 8460 (2020).
[27]N. Mårtensson, E. Sokolowski, and S. Svensson, J. Electron Spectrosc. Relat. Phenom. **193**, 27 (2014).
[28]L. Duò;, M. Sancrotti, R. Cosso, S. D'Addato, A. Ruocco, S. Nannarone, D. Norman, and P. Weightman, Phys. Rev. B **42**, 3478 (1990).
[29]G. E. Franklin, D. H. Rich, A. Samsavar, E. S. Hirschorn, F. M. Leibsle, T. Miller, and T.-C. Chiang, Phys. Rev. B **41**, 12619 (1990).
[30]J. W. Erickson, W. M. Theis, T. Cole, A. K. Green, and V. Rehn, Surf. Sci. **274**, 363 (1992).
[31]P. R. Varekamp, M. C. Håkansson, J. Kanski, D. K. Shuh, M. Björkqvist, M. Gothelid, W. C. Simpson, U. O. Karlsson, and J. A. Yarmoff, Phys. Rev. B **54**, 2101 (1996).
[32]R. L. Anderson, IBM J. Res. Dev. **4**, 283–287 (1960).
[33]H. Kroemer, C R C Crit. Rev. Solid State Sci. **5**, 555–564 (1975).
[34]H. Bae, A. Charnas, X. Sun, J. Noh, M. Si, W. Chung, G. Qiu, X. Lyu, S. Alghamdi, H. Wang, D. Zemlyanov, and P. D. Ye, ACS Omega **4**, 20756 (2019).
[35]R. E. Brandt, M. Young, H. H. Park, A. Dameron, D. Chua, Y. S. Lee, G. Teeter, R. G. Gordon, and T. Buonassisi, Appl. Phys. Lett. **105**, 263901 (2014).
[36]T. Watahiki, Y. Yuda, A. Furukawa, M. Yamamuka, Y. Takiguchi, and S. Miyajima, Appl. Phys. Lett. **111**, 222104 (2017).
[37]M. T. Rizi, M. S. Abadi, and M. Ghaneii, Optik **155**, 121 (2018).
[38]R. E. Brandt, N. M. Mangan, J. V. Li, Y. S. Lee, and T. Buonassisi, J. Appl. Phys. **121**, 185301 (2017).
[39]L. Pan, J. H. Kim, M. T. Mayer, M.-K. Son, A. Ummadisingu, J. S. Lee, A. Hagfeldt, J. Luo, and M. Grätzel, Nat. Catal. **1**, 412–420 (2018).